The Reacting Atmosphere 2

Matthias Ehrhardt *Editor*

Mathematical Modelling and Numerical Simulation of Oil Pollution Problems

Chapter 1
Variability of the Deepwater Horizon Surface Oil Spill Extent and Its Relationship to Varying Ocean Currents and Extreme Weather Conditions

Gustavo J. Goni, Joaquin A. Trinanes, Amy MacFadyen, Davida Streett, María Josefina Olascoaga, Marc L. Imhoff, Frank Muller-Karger and Mitchell A. Roffer

Abstract Satellite observations and their derived products played a key role during the Deepwater Horizon oil spill monitoring efforts in the Gulf of Mexico in April–July 2010. These observations were sometimes the only source of synoptic information available to monitor and analyse several critical parameters on a daily basis. These products also complemented in situ observations and provided data to assimilate into or validate model. The ocean surface dynamics in the Gulf of Mexico are dominated by strong seasonal cycles in surface temperature and mixing due to convective and storm energy, and by major currents that include the Loop Current and its associated rings. Shelf processes are also strongly influenced by seasonal river discharge, winds, and storms. Satellite observations were used to determine that the Loop Current exhibited a very northern excursion (to approximately 28°N) during the month of May, placing the core of this current and of the ring that it later shed at approximately 150 km south of the oil spill site. Knowledge gained about the Gulf of Mexico since the 1980s using a wide range of satellite observations helped understand the timing and process of separation of an anticyclonic ring from the Loop Current during this time. The surface extent of the oil spill varied largely based upon several factors, such as the rate of oil flowing from the well, clean up and recovery efforts, and biological, chemical, and physical processes. Satellite observations from active and passive radars, as well as from visible and infrared sensors were used to determine the surface extent of the oil spill. Results indicate that the maximum and total cumulative areal extent were approximately 45×10^3 km^2 and 130×10^3 km^2, respectively. The

G.J. Goni (✉) · J.A. Trinanes
Atlantic Oceanographic and Meteorological Laboratory, National Oceanic and Atmospheric Administration, 4301 Rickenbacker Causeway, Miami, FL 33149, USA
e-mail: gustavo.goni@noaa.gov

J.A. Trinanes
Rosenstiel School of Marine and Atmospheric Science, Cooperative Institute for Marine and Atmospheric Studies, University of Miami, 4600 Rickenbacker Causeway, Miami, FL 33149, USA
e-mail: joaquin.trinanes@noaa.gov

M. Ehrhardt (ed.), *Mathematical Modelling and Numerical Simulation of Oil Pollution Problems*, The Reacting Atmosphere 2, DOI 10.1007/978-3-319-16459-5_1

largest increase of surface oil occurred between April 22 and May 22, at an average rate of 1.3×10^3 km^2 per day. The largest decrease in the extent of surface oil started on June 26, at an average rate of 4.4×10^3 km^2 per day. Surface oil areas larger than approximately 40×10^3 km^2 occurred during several periods between late May and the end of June. The southernmost surface oil extent reached approximately 85°W 27°N during the beginning of June. Results obtained indicate that surface currents may have partly controlled the southern and eastern extent of the surface oil during May and June, while intense southeast winds associated with Hurricane Alex caused a reduction of the surface oil extent at the end of June and beginning of July, as oil was driven onshore and mixed underwater. Given the suite of factors determining the variability of the oil spill extent at ocean surface, work presented here shows the importance of data analyses to compare against assessments made to evaluate numerical models.

J.A. Trinanes
Technological Research Institute, University of Santiago de Compostela Laboratory of Systems, Campus Vida 15782, Santiago, Spain

J.A. Trinanes
National Environmental Satellite Data and Information Service, CoastWatch, National Oceanic and Atmospheric Administration, 5200 Auth Road, Camp Springs, MD 20746, USA

A. MacFadyen
Office of Response and Restoration, Emergency Response Division, National Oceanic and Atmospheric Administration, 7600 Sandpoint Way, Seattle, WA 98115, USA
e-mail: amy.macfadyen@noaa.gov

D. Streett
National Environmental Satellite Data and Information Service, Office of Satellite and Product Operations, National Oceanic and Atmospheric Administration, Camp Springs, MD 20746, USA
e-mail: davida.streett@noaa.gov

M.J. Olascoaga
Rosenstiel School of Marine and Atmospheric Science, Ocean Sciences Department, University of Miami, 4600 Rickenbacker Causeway, Miami, FL 33149, USA
e-mail: jolascoaga@rsmas.miami.edu

M.L. Imhoff
Pacific Northwest National Laboratorys Joint Global Change Research Institute, 5825 University Research Court, College Park, MD 20740, USA
e-mail: Marc.Imhoff@pnnl.gov

F. Muller-Karger
College of Marine Science, University of South Florida, 140 7th Avenue South, St. Petersburg, FL, USA
e-mail: carib@usf.edu

M.A. Roffer
Roffers Ocean Fishing Forecasting Service, Inc., 60 Westover Drive, West Melbourne, FL 32904, USA
e-mail: roffers@bellsouth.net

1.1 Introduction

A major crude oil spill occurred following an explosion aboard the Deepwater Horizon (DWH) drilling platform in the northern Gulf of Mexico (GOM) on April 20, 2010. This spill differed from other significant oil spill events in that it was the largest accidental oil spill in US history [19]. It occurred in the open ocean at a depth of 1500 m, and both oil and dissolved oil had the potential to affect distant areas of the GOM at the ocean surface and subsurface. This spill occurred in a significant ecosystem that supports major fisheries, and numerous endemic and migrating populations of fish, reptiles, birds, marine mammals, plankton and various sensitive benthic communities. A very large effort was initiated and sustained by the scientific and operational communities of the nations bordering the GOM to assess the extent to which oil was spreading. The oil continuously entered the deep GOM between late April and the time of final capping on July 15, 2010, spreading by means ocean and wind forcing at the surface and subsurface [16].

A suite of satellite-derived products and analyses were developed and generated in real time to address the need to observe the synoptic scales of the spill which is critical to assess numerical model outputs. The satellite data and products were provided through joint government, academic, and private sector partnerships to help the operational community with its response efforts to task and direct oil-spill clean-up and recovery-related efforts. These satellite data and their derived products served as a critical complement to observations collected from field programs and, at times, provided the only available observations and products to perform rapid estimates of a number of environmental parameters over large geographic areas. For example, these observations proved to be critical for real-time analysis and assessment of the GOM conditions to: (a) Monitor the extent and variability of the oil spill at the ocean surface; (b) Assess the surface circulation that could create surface oil pathways and boundaries to the surface oil extent; (c) Monitor surface winds that could force the motions of oil and water; and (d) Initialize and validate numerical models. This chapter provides a review of the extent of the surface oil and of the upper ocean dynamic conditions (a through c) as observed using a suite of satellite observations, analyses, and products, during the 2010 DWH oil spill.

Satellite and in situ observations were used to monitor the variability of the extent of the surface oil. Aircraft overflights with observers and a wide collection of sensors, such as side-looking airborne radar and infrared and hyper-spectral sensors, were used to complement and validate the satellite observations and to provide additional details about oil location, oil thickness, and areal coverage. Some of these datasets will take years to process to fully exploit their information content. The large areal extent of the spill, however, precluded aircraft mapping of the entire surface oil area. Therefore, the integration of aircraft and satellite data provided an overview of the spill that neither observational platform could achieve alone. In addition, satellite monitoring was also used to assess whether and how upper ocean dynamics were conduits for the long distance transport of water and oil particles to areas far removed from the oil spill source. This was particularly important early in the spill. There were

concerns about oil becoming entrained in the Loop Current (LC) and in Loop Current Rings (LCR). Although existing methodologies [11] and numerical model efforts in general allow estimating the upper ocean thermal structure from satellite altimetry observations, research cruises still supply needed critical in situ information used to validate and assess satellite ocean current observations and to provide a suite of subsurface data that could not have been obtained otherwise [30, 31] to perform a correct water mass analysis.

Trajectory models, initialized and validated by satellite observations, also played a key role in contingency planning and determining the likelihood water and oil particles located at or in the vicinity of the oil spill site to reach remote regions, such as the west Florida shelf, Florida Keys, etc. [14, 17]. Northern GOM waters have been observed in these downstream regions, such as the Florida Straits via the LC [7, 23, 24]. In addition, historical surface drifter trajectories indicated that material particles travelling near the oil spill site had the potential to enter the North Atlantic [30]. However, oil did not reach the western-central or southwest coast of Florida, consistent with earlier expectations of [35], who examined satellite-tracked drifter trajectories in this region. The flow regime of this region minimizes the cross shelf transport in the West Florida Shelf [13, 28]. This region, however, shows seasonal variation [26] that can be related to the northward excursions of the LC, which extends from 24°N to 28°N. Specifically, the circulation in this region would allow surface materials in the GOM to be closer to the shoreline when the edge of the LC reaches a maximum northern excursion, and farther away when the LC is at its southernmost location [6, 26, 28].

When the DWH incident began on April 20, 2010, the LC was in its northern extension, reaching approximately 27.5°N, still south of the wellhead location (88.36°W, 28.73°N). Numerical models initialized with in situ and satellite observations reflecting these conditions were used to calculate the trajectories of synthetic Lagrangian water particles deployed in the oil spill site to examine potential transport pathways arising from ocean currents. A numerical methodology based on Finite Time Lyapunov Exponents, which is an averaged measure of the separation rate of initially nearby fluid particle trajectories, was used to identify regions that could act as barriers not allowing the intrusion of waters near the west Florida coast and to estimate potential oil pathways at the surface. Numerical model-derived particle trajectories exhibited a number of pathways with a potential to reach areas beyond the oil spill site, to be carried into the southern GOM, and to enter into the Florida Current and North Atlantic Ocean at the surface (Fig. 1.1) and subsurface. Depending on the decay rate assigned to these particles, some could reach remote regions, although with a very low density or probability [1].

Real-time evaluation of surface current fields mostly derived from satellite observations became a critical component of the monitoring effort. The complexity of these fields is enhanced by the mechanisms involved in the separation of rings from the LC [33], which usually occur at different times at surface and subsurface. The separation of the LCRs at the subsurface is only verifiable with in situ measurements as satellite observations are limited to surface parameters. The spatial resolution of the fields derived from multiple satellites became especially important for real-time

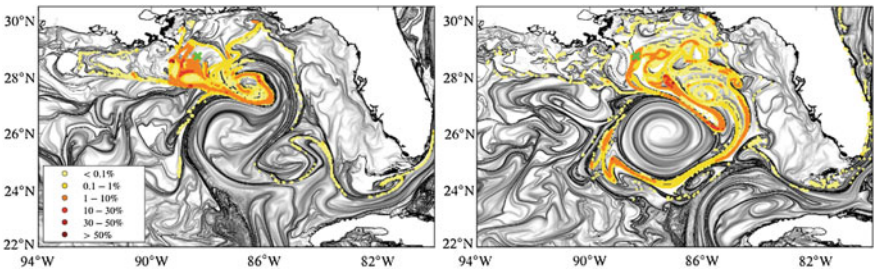

Fig. 1.1 Finite Time Lyapunov Exponents fields used to evaluate the path of particles at the surface for the ocean surface conditions on (*left*) May 20 and (*right*) June 2, 2010. Convoluted bands of most intense *black tones* indicate attracting Lagrangian Coherent Structures, which delineate the pathways of the particles. In a numerical experiment, 10,000 water particles were released daily near the location of the Deepwater Horizon oil well starting on April 20 and finishing on (*left*) May 20 and (*right*) June 2, 2010. The water particle density denoted by colours *yellow* (low values) to *orange* (higher values) is expressed as percentage of the daily discharge in 1/25 × 1/25 bins. No particles were found to enter the West Florida Shelf and only a minimal fraction entered into the Loop Current and Florida Current systems

mapping of mesoscale features present in the GOM, which are frequently observed along the periphery of the larger features, including the LC. The complex surface current field, which could not be measured by one satellite alone, necessitated continuous monitoring of the highly variable dynamic conditions of the upper ocean and was accomplished by using a combined analysis of satellite together with in situ observations and numerical modelling.

This work shows the importance of a combined analysis of observations and numerical modelling. The goal of this chapter is to present results obtained from this combined analysis on the link between the variability of the surface oil extent with synoptic surface ocean currents and winds during the DWH event. This chapter is organized as follows. The data and methods used to identify surface oil and surface currents are presented in Sect. 1.3. Results obtained from a suite of hydrographic and satellite observations and from numerical models outputs are shown in Sect. 1.4 detailing the evolution of the LC system during April–August 2010 from satellite fields that were used to identify the main ocean features and to explore potential links between ocean dynamics and the oil spill extent. Section 1.5 summarizes the main conclusions of this chapter.

1.2 Upper Ocean Dynamics in the Gulf of Mexico

The upper ocean circulation in the GOM is characterized by the excursions of the LC, which irregularly sheds anticyclonic rings that travel in a northwest direction into the GOM. The LC forms an intense anticyclonic flow, which expands north westward [9] and can extend northward into the GOM to 28°N, in the vicinity of the

shelf break of the northern portion of the West Florida Shelf (WFS) at about 250 km off the coast [21]. The northern intrusions of the LC may occur in any season with periods ranging from 6 to 17 months, but tend to be more frequent during the spring months [15, 20, 34]. Results derived from hydrographic and satellite observations show that large, warm-core anticyclonic rings, referred to as LCRs, are usually shed from the LC and propagate westward at mean translation speeds of approximately 4 km/day and have mean lifetimes of days to around a year [12, 23, 34, 37]. These LCRs have radii of about 150 km and may reach depths of 800 m [25].

1.3 Main Data Sets and Methods

1.3.1 Surface Oil Extent

During the DWH response, the NOAA Office of Response and Restoration's Emergency Response Division provided daily forecasts of the movement of surface oil, predicting movement over 24, 48 and 72 h intervals [17]. In previous incidents, the primary dataset used to initialize oil distributions for modelling purposes was derived from overflight observations, which would ideally delineate the oil slick boundary and provide detailed descriptions of the distribution and percent coverage of differential oil thickness. However, even with multiple overflights per day being conducted from several locations along the Gulf Coast, the areal magnitude of this oil spill made it difficult for visual overflight observations to provide a comprehensive and complete picture of the oil distribution.

Two primary data types were used to monitor oil at the ocean surface from space: (a) surface roughness from microwave radiation; and (b) Visible and Near Infrared (VNIR) data. By the second week of the incident, the experimental Marine Pollution Surveillance Reports (MPSRs) provided by NOAA National Environmental Satellite, Data, and Information Service (NESDIS) were an integral dataset used in the model initialization. These analyses [32] provided an outer boundary for the extent of the surface oil in a time frame that allowed use by the command posts to direct operations, including overflights. The MPSRs delineated the extent of surface oil using satellite imagery from both active and passive sensors and from other supplementary information such as overflights and in situ observations. During the incident, the MPSRs were rapidly made available, providing information about the surface oil location after each satellite pass. The MPSRs were used in this study in combination with surface current fields to examine potential links between the GOM surface dynamics and the surface oil extent (Fig. 1.2).

Synthetic Aperture Radar (SAR) sensors have been the traditional approach used for assessing surface roughness for oil spill detection [2] since they are all-weather, day and night, active sensors that emit microwave pulses and measure the backscatter radiation reflected by the sea surface, which is a function of the sea surface roughness. The constellation of space-borne SAR sensors (onboard satellites such as

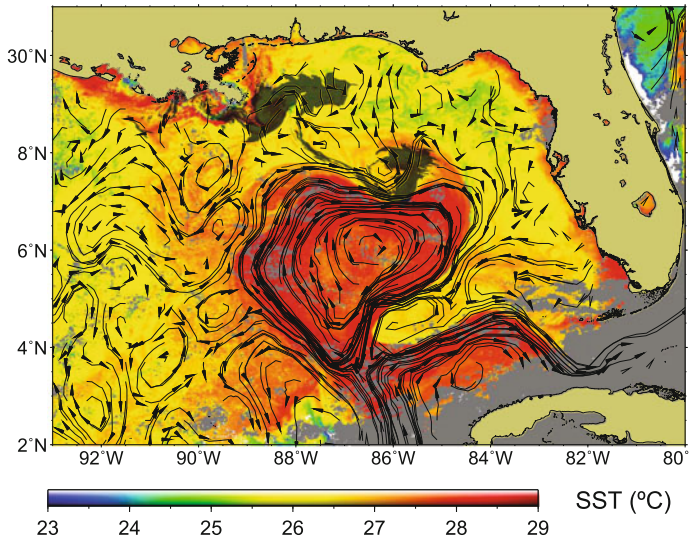

Fig. 1.2 Sea surface temperature (SST) composite for May 20, 2010. The detailed SST features can be used as a proxy for inferring surface circulation and to complement the altimetry derived surface current fields. The main features observed here are the anticyclonic Loop Current and the soon to be detached Loop Current ring, which have higher SST than their surrounding waters. The *arrows* correspond to a coincident geostrophic current velocity field computed using 11 days of satellite altimeter data centered on May 15. The surface oil extent, the two large linked areas shown in *dark green* and centered at 29°N and 27°N, corresponds to May 20–21; it is bounded to the south by the circulation of a Loop Current ring, and it retroflects to the north following the edge of a cyclonic eddy

Envisat, RadarSat 1&2, and TerraSAR-X) provided an almost daily coverage of the GOM region and were essential inputs for monitoring the extension and movement of the oil spill and, consequently, for creating the MPSRs.

On the other hand, VNIR and Infrared data are obtained from multiple passive sensors, such as the Advanced Very High Resolution Radiometer (AVHRR, on satellites within the Polar Orbiting Environmental Satellites constellation), the Moderate Resolution Imaging Spectroradiometer (MODIS on NASA Terra and Aqua satellites), MEdium Resolution Imaging Spectrometer (MERIS, on the Envisat satellite), the Advanced Spaceborne Thermal Emission and Reflection Radiometer (ASTER, on Terra), and the Multi-angle Imaging SpectroRadiometer (MISR, also on Terra) (Fig. 1.3). MODIS data were used primarily for broad-scale surface mapping, spill trajectory and ocean circulation model parameterization, and marine ecological impact analysis [16, 18, 22]. The thermal infrared bands of the ASTER instrument, MODIS and AVHRR were used to detect temperature differences, which in some cases could be caused by the difference between seawater temperature and the colder freshly emerging oil. The oil slick appeared in MODIS pseudo colour images differently depending on many different factors, including whether the oil was in

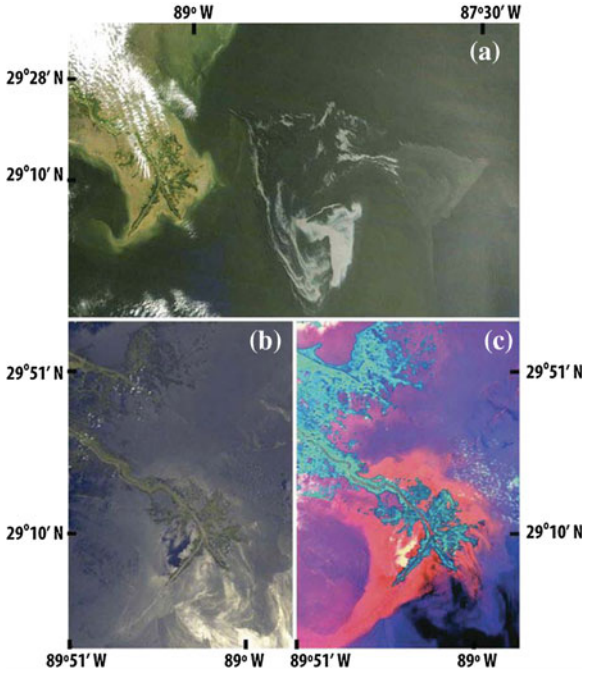

Fig. 1.3 **a** Oil slick as seen in a Terra MODIS visible-near IR image, distinguishable because of its a pale swirl in the darker seawater of the Gulf of Mexico just south of the Mississippi Delta on May 1, 2010; **b** MISR true colour image for May 17, 2010; **c** MISR multi-angle composite acquired on the same date that separates the oil spill (*black* and *dark blue*) from specular reflections

the sunglint pattern of the near-noon collections or outside (Fig. 1.3a). Oil at the sea surface can have a higher or lower reflectance than the surrounding seawater across the visible and near IR bands [8, 10]. As a result, these images were used to measure the surface area and edges of the spill and the direction of flow over time. The capabilities of MISR enhanced the difference in brightness by reducing sun glint, and the use of textural classifiers increased mapping accuracy by using single images. The MISR images (Fig. 1.3b, c) demonstrated how far the oil had dispersed on the sea surface around the Mississippi Delta. The MISR combines images taken at different angles into a single computerized colour image that distinguishes surface oil from seawater and silt. Oil is shown in black and dark blue colours, while silt from the Mississippi is shown as red, orange, and pink colours. Because oil has a different thermal inertia than seawater, multi-temporal thermal data from satellite sensors, such as MODIS or ASTER, were examined and used to further reduce the error in oil slick identification. Interpretations of these image types were verified by imagery derived from SAR images and from overflights.

The operational preparation of the MPSRs involved satellite imagery as well as ancillary data such as surface currents and winds. The different sources of radar and

VNIR imagery mentioned above were all used within an operational context during the DWH incident.

Due to the large area of the spill, view angle effects, and the limited size of the areas imaged by many of the satellites used, daily repeat satellite coverage of the entire spill was sometimes incomplete. To partly address the limitation of individual satellite passes, each daily estimate of the area time series used in this study corresponds to a three-day average. The variability in this time series may be due to several factors, including wind forcing, ocean dynamics, changes in the flow rate of oil from the well, recovery efforts (e.g. skimming efforts), oil washing ashore, and lack of measurements due to cloud coverage. A limitation of the MPSRs was the inability to differentiate a thin sheen from very thick oil. Also variations in the wind speed affect the interpretations of the satellite data. For example, high winds affect both the true and apparent extent of oil coverage. High surface wind speeds over the slick tended to decrease satellite-derived surface oil extent because wind and wave forcing caused oil droplets to become increasingly dispersed into the surface mixed layer and, consequently, become undetectable by satellite. Rough seas and deep convection caused oil to be difficult to view in satellite imagery. In addition, rough seas and high winds also enhanced natural dispersion, which resulted in apparent reduction of the surface oil extent. On the other hand, during calm wind periods, relatively thin oil sheens on the sea surface could be detected using satellite observations. Persistent (three days or longer) limitations in satellite coverage or optimal viewing conditions also affected the assessment of the extent of the detected surface oil, tending to create an underreporting of the amount of oil coverage. In addition, the satellite techniques presented here did not show onshore oil or, generally, oil in wetlands. Therefore, any oil that washed ashore or moved into the wetlands did not appear in the MPSRs and, thus, decreased the actual surface oil extent. At any rate, the detection of oil onshore and in wetlands falls outside the scope of this chapter.

The final MPSR analysis product was an outline of an ‘anomaly’ presumed to be oil. In fact, the surface oil varied substantially in type, thickness, concentration, and percent coverage. Identification and prediction of the location of thicker oil is of crucial importance to the response, as this oil may be recoverable via skimmers or targeted for in situ burning, and also poses the greatest threat to shorelines. Thinner and patchy relatively small oil slicks and lower concentrations of oil are also important in evaluating possible effects on the ecosystem. False-positives were also an issue, with transparent, presumably biological, sheens and patches of sargassum frequently erroneously identified as oil. Therefore, satellite analysis was critical to directing overflights, and overflight observations provided essential feedback for the validation of the satellite analysis. Ultimately, satellite and overflight data were used daily to initialize the surface oil distribution for modelling purposes by overlaying analyses from individual satellite passes and observations from multiple overflight tracks to create a time-dependent surface oil distribution.

The response to the DWH incident also demonstrated the benefits of combining SAR and VNIR, especially the latter under sunglint conditions, when oil slicks increase the specular reflectance of the sea surface, and the oil covered areas have more brightness than the regular oil-free ocean surface, making it easier to extract

information on the extent of the oil at the surface. A potential third approach using sea surface temperature (SST) observations was also explored during the monitoring efforts and showed good potential for analysis of changes in surface oil extent. No results using this type of analysis are presented in this chapter because they fall beyond the scope of the work carried out during the oil spill monitoring efforts. However, SST observations were also used to classify water masses with different and often unknown concentrations of oil as part of evaluating the possible pathways for dispersal.

1.3.2 Surface Currents

After the Seasat and Geosat satellites proved the concept that ocean currents could be monitored and studied from space using radar, a number of space-based altimeters have flown beginning in late 1992. Data obtained from an altimeter onboard a satellite, with the proper atmospheric corrections, represents the distance between the satellite and the sea surface, and indirectly serves to estimate the sea surface height anomaly (SSHA) along the altimeter groundtracks. The observations provided by altimeters are accurate estimates of the SSHA away (∼50 km) from coastal zones [3], and are referenced to a mean sea height, which may be generated from historical hydrographic observations and/or numerical models during a period of several years. This process smears out mesoscale ocean features smaller than approximately 100 km and those that move at speeds faster than a few kilometers per day.

During the DWH oil spill, fields of surface circulation were constructed using data from various sources, both in situ and remote. Results presented here focus on those fields obtained at the time of the oil spill using real-time satellite altimetry observations. However, this work presents results that use delayed-time altimetry observations, which generally become available with a several month delay. Two main data sets were used to derive the upper ocean circulation from satellite altimetry: (a) delayed-time altimetry-derived sea surface height (SSH) anomaly along-track data from the Jason-2 and Envisat satellite missions, whose groundtracks are separated by approximately 3 and 1 degrees in longitude, and are repeated approximately every 10 and 35 days, respectively; and (b) a synthetic mean dynamic topography or sea surface height [29]. Horizontal gradients of regularly gridded SSH fields derived from the alongtrack satellite altimetry data were used to estimate daily surface geostrophic currents following a well-established methodology [4]. The spatial gradients of these geostrophic currents were then used to determine the location of the fronts associated with the cyclonic and anticyclonic features, such as the LC, rings and eddies. Results regarding the separation of the LCR from the LC, based on these surface currents alone, may often differ from those obtained from satellite-derived SST estimates, as the boundaries of the mesoscale features observed from dynamic and temperature fields may not necessarily coincide. The fields of surface currents are used in this work to understand and assess how ocean dynamics delineate the outer boundary of the oil extent.

Fields of altimetry-derived surface currents and associated frontal regions were used operationally by the NOAA Office of Response and Restoration to monitor the upper ocean dynamics. The real-time fields produced during the oil spill event are located at www.aoml.noaa.gov/phod/dhos. Altimetry observations have the advantage that they are available year-round and are not affected by the near uniform SST values often observed over the GOM during the summer months. The altimetry fields also have the benefit of not being subject to cloud contamination. However, they cannot provide the fine spatial and high temporal resolution to resolve surface features obtained from satellite-derived fields of SST and ocean colour. Since altimetry fields are constructed using the alongtrack satellite data, which may not necessarily run along or across the region of LCR detachment, the exact date of detachment of a LCR as seen from altimetry observations is only approximate.

1.3.3 Surface Features from Sea Surface Temperature and Ocean Colour

Satellite observations of SST and ocean colour were used jointly to determine the size and location of smaller mesoscale features that satellite altimetry fields cannot observe or properly resolve. These smaller features were detected by adjusting the contrast of the images and outline in the image. Ocean colour data were particularly useful for mapping surface ocean circulation features during the summer months, when SSTs in the Gulf of Mexico (GOM) have relatively weak gradients compared with the winter months [24]. Ocean colour observations from MODIS, SeaWiFS (on SeaStar) and MERIS were routinely used to study regional dynamics. The gradients of ocean colour and derived surface chlorophyll concentration make these data particularly useful in the GOM.

Several passive satellite sensors were available to estimate SST by measuring thermal infrared (IR) and microwave radiation emitted by the ocean. During the DWH event, SST imagery collected using IR sensors, allowed researchers to make inferences about the distribution of surface features and frontal zones that could have been associated with different water masses in the GOM. The satellite sensors used in this study were the various AVHRR sensors, MODIS, and the European Advanced Along-Track Scanning Radiometer (AATSR, onboard Envisat). The 6 km resolution SST fields from the geostationary GOES-12 were also used to obtain coverage when clouds were present by virtue of its sub-hourly sampling. Of significance is that it is still not understood how oil present at the surface of the ocean affects the emissivity of the IR radiation, whether SST observations within oil-covered waters were accurate or not, or whether this signature changed with patchiness in the oil or weathering of the surface slicks. During the oil spill event, maps of SST (Fig. 1.2), ocean colour fields, ocean frontal zones and derived circulation were routinely prepared by ROFFSTM, NOAA, and other laboratories to monitor the upper ocean conditions. Some of these

fields can be found at www.aoml.noaa.gov/phod/dhos and http://www.roffs.com/research-environmental/deepwater-horizon-rig-oil-spill-monitoring.

1.4 Analysis and Discussion

1.4.1 Surface Oil Spill Extent

The extent of the surface oil was primarily estimated and analysed from blended satellite observations as explained in Sect. 1.3.1. The daily MPSRs were used to assess the daily extent of the surface oil and to link their temporal and spatial variability to the surface current fields (Fig. 1.4). The time series of the areal extent of the surface oil (Fig. 1.5b), as obtained from the MPSRs, had a mean value of approximately $20 \times 10^3\,km^2$ and exhibited large temporal variability. An evaluation of these reports indicates that the total cumulative area of oil detected over the open water during the 87 days of the oil spill between April and August 2010, was at least $130 \times 10^3\,km^2$ (Fig. 1.5c). The area covered by surface oil for more than 40 days was slightly smaller than $10 \times 10^3\,km^2$. The surface oil extent was at a maximum ($40 \times 10^3\,km^2$) between approximately May 14 and June 29, 2010, with one noticeable minimum value of less than $15 \times 10^3\,km^2$ around June 6, 2010.

Between April 22 and May 22, 2010, when the first maximum in surface area extent occurred, the surface oil extent increased at an average rate of $1.3 \times 10^3\,km^2$ per day. Areas larger than $40 \times 10^3\,km^2$ were observed during May 20–25, June 16–22, and June 24–27, 2010 (Fig. 1.5a). On the other hand, the areal extent of the surface oil decreased between June 27 and July 5 at a rate of $-4.4 \times 10^3\,km^2$ per day, a rate approximately three times faster than the increase rate during April 22–May 22, 2010. Significant progress had already been made by responders in dispersing, burning, or recovering the oil during this time period. The magnitude of the June 2–6, 2010 apparent decrease of approximately $-20 \times 10^3\,km^2$, was partly due to particularly limited satellite coverage during this time, although a true decrease in oil extent cannot be ruled out.

Wind fields used in the analysis of this work correspond to the 0.25° surface wind grid from NCEP Reanalysis-2 data [36]. The prevailing winds over the GOM during the oil spill were from the southeast and with an average speed of approximately 5 m/s, while winds from other directions were, in general, weaker, with average speeds around 2 m/s (Fig. 1.5a).

By the end of June, high winds, rough seas, and distant thunderstorm activity occurred as Hurricane Alex moved through the southwestern GOM, affecting conditions in the spill area, and causing satellite analysis to underreport the surface oil coverage during this relatively short time period. During the passage of the strong southeasterly winds associated with Hurricane Alex, the daily average wind speed at the oil spill site was approximately 7.4 ± 2.5 m/s, while outside this time period the daily average wind speed was approximately 4.1 ± 2.3 m/s (Fig. 1.5a). The

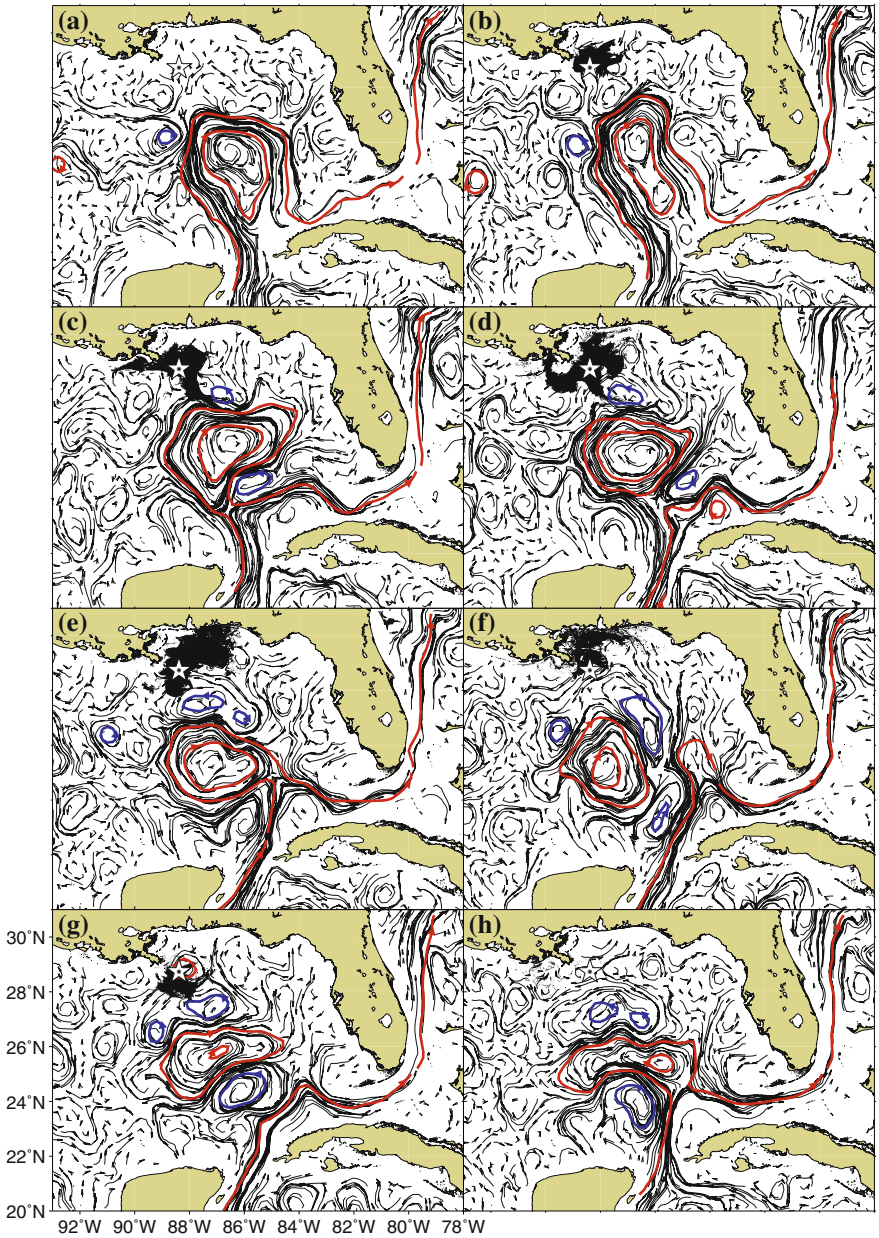

Fig. 1.4 Maps showing surface oil coverage (regions in *black*) for eight selected days in 2010 as obtained from five-day (centered on the referenced day) product superimposed on the altimetry-derived surface currents (*grey arrows*), showing selected sea height contours that are associated with the main mesoscale cyclonic and anticyclonic features (*blue* and *red lines*, respectively). The *star* placed at 88.36°W, 28.73°N, shows the location of the Deepwater Horizon oil spill site. **a** APR 15. **b** MAY 01. **c** MAY 15. **d** JUN 01. **e** JUN 15. **f** JUL 01. **g** JUL 15. **h** AUG 01

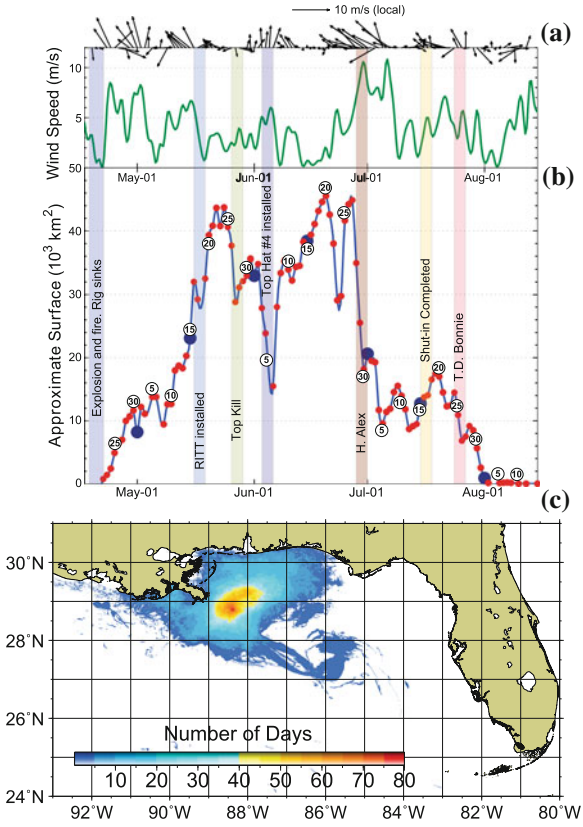

Fig. 1.5 **a** Time series of the wind direction and intensity. **b** Time series of the daily area (in 10^3 km^2) covered by surface oil as obtained from the Marine Pollution Surveillance Reports (MPSRs). A three-day running test on the presence of oil was applied to minimize the impact of partial satellite coverage. *Red circles* denote the estimated values, while the *blue line* shows the results of a cubic spline fit to these values. The numbers in the *white circles* indicate the day of the month. The *blue circles* indicate the dates in which maps of surface currents and surface oil spill extent are shown in Fig. 1.4. **c** Cumulative oil area during April–August, 2010. Colours indicate the number of days the oil slick was present in the daily MPSRs

predominant winds during Alex had the potential to cause the oil to move and concentrate in more westerly locations, enhance dispersion, or simply drive oil ashore predominantly along the barrier islands of the Mississippi Sound. The areal extent of the oil immediately after the passage of Hurricane Alex exhibited a reduction of approximately 28×10^3 km^2, a value of more than half the pre-hurricane surface oil extent (Figs. 1.5b and 1.6). Winds from Tropical Depression Bonnie on July 24–25, 2010, contributed partly to this temporary apparent decrease in surface oil extent.

The limits of the main surface oil area extended south to approximately 27°N 86°W during May 16–28, 2010, and east to approximately 85°W 28°N during May

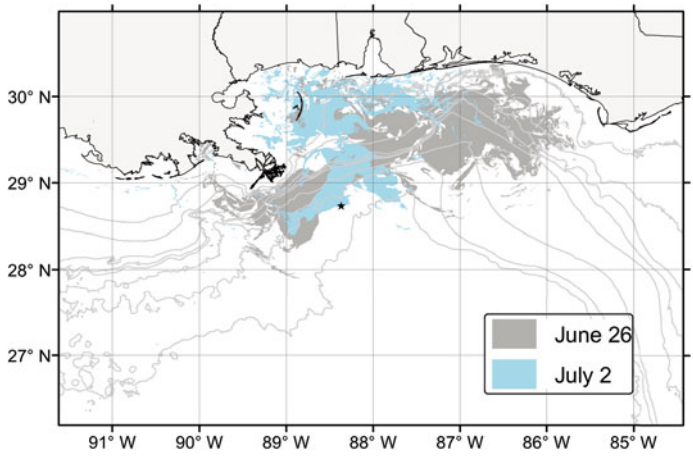

Fig. 1.6 Map showing two areas of extent of the surface oil obtained from the NOAA National Environmental Data and Information Services experimental Marine Pollution Surveillance Reports (MPSR) products. These maps correspond to pre- (June 26, 2010, in *dark gray*) and post- (July 2, 2010, *light blue*) Hurricane Alex. Average surface SE winds of 7.4 m/s during this time period contributed to the reduction of the surface oil extent. *Gray lines* indicate bathymetry contours of 25, 50, 100, 200, 500, 1000, and 2000 m

19–23, 2010. These locations only reflect the extent of surface oil identified in more than one report and as a single continuous area. In addition, smaller areas of potential surface oil slick were reported in the MPSRs. However, large uncertainties existed in their identification and location, and their confirmation therefore relied on visual inspection by overflights. These areas, which extended as far south and east as 24.1°N and 83.0°W, were generally not sampled, and very few of them were confirmed by overflights. Additionally, a relatively very small amount of this oil could have originated in natural seeps or other anthropogenic sources. Observations indicated that these areas consisted of transparent sheens, which may have been very thin oil (∼40 nm) or may have been biological in origin (natural sheening of sargassum). For example, a slick detected approximately 160 km southwest of Tampa, Florida, was confirmed as a transparent sheen by a C130 overflight conducted on June 2, 2010. No further visual analysis or sampling was carried out at later dates in this region. In addition, there were several short-lived slicks detected around the LCR that reached south of 27°N between 85°W and 87°W at the end of May and beginning of June. However, they were not confirmed by overflights or by in situ observations. These could have been formed due to ephemeral surface convergence as sequential image analysis suggested that it was possible for DWH oil to have reached this area. However, compared with the other areas, especially those with recoverable oil, these areas contribute to less than 5 % of the total surface oil spill area.

In addition to surface currents, the surface oil extent depended on other factors, such as the rate of oil flowing from the well, which on average was estimated to range between 50,000 and 70,000 barrels per day [19]. A suite of recovery efforts was

done (http://energy.gov/downloads/key-events-timeline) including the Riser Insertion Tube Tool (RITT) to recover oil from the riser to a surface ship; the pumping of heavy drilling fluids into the blowout preventer to restrict the flow of oil before sealing it permanently with cement (referred to as "top kill"); and the installation of a piece of equipment over the flowing well after the riser was removed to capture hydrocarbons so that they could be collected at the sea surface (referred as to top hat #4). The time line of these efforts with relation to the oil spill extent at the surface is included in Fig. 1.5.

1.4.2 Surface Ocean Circulation

Throughout the response it was critical to provide an early warning of possible threats to remote regions from surface oil entrained in the northern extension of the LC. The importance of identifying periods of time with northern extensions of the LC or LCR is that they had the potential to create direct pathways between the northern GOM and the LC and surrounding Gulf of Mexico including the West Florida Shelf and Florida Keys. In addition, surface mesoscale dynamics also exhibited a close relationship between the extent and shape of the surface oil during much of the DWH event. The complex surface circulation in the GOM, characterized by the LC and the presence of cyclonic and anticyclonic eddies (Figs. 1.1, 1.2 and 1.4) was assessed by the joint analysis of numerical model outputs and satellite observations. Hydrographic data and numerical models were used to assess the connectivity of the LC with the LCR below the surface [30, 31].

The front or core of the LC and rings were identified in terms of the highest geostrophic velocity values, which correspond to the highest horizontal gradient in SSH which for the LC is approximately 0.005 m/km. Values of SSH associated with these maximum gradients ranged from 0.020–0.050 m for anticyclonic features and from 0.00–0.020 m for cyclonic features. The altimetry-derived fields of geostrophic velocity were complemented by a limited number of available in situ observations from hydrographic cruises that were specifically geared towards understanding the connectivity between the LC and the LCR at depth [30]. Results regarding the separation of a LCR from the LC, based on surface currents alone, may also differ from those obtained from SST estimates, as the mesoscale features derived from dynamic and temperature fields may not necessarily coincide.

On April 15, 2010, before the oil spill occurred, the LC presented its northern limit at approximately 27°N with some of its circulation contained in an anticyclonic motion centred at 25.5°N inside the LC (Fig. 1.4a). At this time the LC northern boundary was translating to the north at ~40 km/week. When the oil spill occurred on April 20, 2010, the northern limit of the LC was located at around 27.5°N, approximately 190 km from the spill site. The LC reached its northernmost excursion of approximately 28°N during the first half of May, at approximately 150 Km from the oil spill site. Therefore, according to data analysed in this work, this is the closest distance between the LC/LCR system with the oil spill site. Around mid May, the

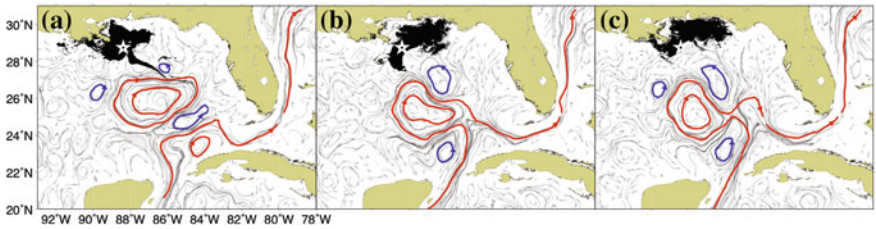

Fig. 1.7 Maps showing the areal extent of surface oil (regions in *black*) for three different dates (May 20, June 20, and June 27, 2010), as obtained from the 5-day (centred on the referenced day) experimental Marine Pollution Surveillance Reports (MPSR) product. These areas are superimposed on the altimetry-derived surface currents (*grey arrows*), showing selected sea height contours that are associated with the main mesoscale cyclonic and anticyclonic features (*blue* and *red lines*, respectively). The star placed at 88.36°W 28.73°N, shows the location of the Deepwater Horizon oil spill site. **a** MAY 20. **b** JUN 20. **c** JUN 27

surface oil began to spread and attained its first maximum of areal extent (Fig. 1.7b), approximately reaching its southernmost location at 27°N (Fig. 1.4c). At this time, the southern boundary of the main surface oil area, located at approximately 27°N, followed the shape of the northern edge of the large LCR and extended south and east of the small cyclonic eddy centred at approximately 86.5°W 27.5°N as revealed by satellite-derived surface currents (Fig. 1.4c) and pathways of water particles using numerical modelling (Fig. 1.1). However, these southern extensions of the surface oil extent did not necessarily correspond to the maximum oil extensions, except for mid May. These results highlight the close link between surface ocean dynamics and the surface oil extent.

The pathways and boundaries of the LC and LCRs were also partly defined by Lagrangian Coherent Structures (LCSs) patterns formed by passive tracers, e.g. [5], which control transport and mixing. These features are revealed using, for example, synoptic fields of sea surface temperature and ocean colour, or can be extracted from current velocity fields using Lagrangian techniques. For example, LCSs can help to explain the shape of the surface oil extent for May 20, 2010 (Fig. 1.1; [27]), which is one of the dates when a maximum of surface oil extent occurred (Figs. 1.4c and 1.5b). At the time of the oil spill, the dynamical conditions of the LC exhibited a marked northern excursion with the potential of GOM waters to get closer to the West Florida Shelf. Numerical experiments carried out in which water particles were released at the surface near the oil spill site indicate that none of the synthetic water particles made their way onto the shelf (Fig. 1.1). This is consistent with the presence of an unbroken barrier that partially inhibits transport across the shelf. In addition, numerical model experiments revealed that almost no particles ($<0.1\,\%$) reached the coastal waters near the Florida Keys (Fig. 1.1). The lack of agreement sometimes found between this type of study and simulated oil distributions may be partly attributed to neglecting the non-conservative behaviour of oil in the simulations.

After reaching its northernmost location in mid-May, the LC began shedding a LCR, aided in part by its interaction with the cyclonic eddy centred near 85°W 25°N

(Fig. 1.4d). On June 2, 2010, surface oil was observed 160 km SW of Tampa, Florida. The LCSs corresponding to this day indicated that the transport barrier was broken and closer to the shoreline on the West Florida Shelf (Fig. 1.1), which partly justified the presence of oil in this area. The LCR was shed and remained unattached from the LC at the surface until approximately June 14, 2010. Surface drifter trajectories confirmed that there was no surface connectivity between the LCR and the LC. During one hydrographic cruise, four surface drifters were deployed at approximately 84°W 26°N, outside the LC and LCR system, where tar balls had been observed. Their trajectories crossed the region between the LC and LCR at 84.5°W 24.5°N on June 13, 2010, (Fig. 1.8), providing an indication that these two features were probably not connected, and that there was no direct connectivity between the LCR and the LC, at least at the surface. However, by June 15, 2010, the LCR had reattached to the LC, as observed by altimetry (Fig. 1.4e) and SST observations. Consequently, from June 13–28, 2010, there was a direct path of waters from the anticyclonic ring into the LC.

Satellite-tracked surface drifting buoys trajectories (Fig. 1.8) were used to assess the upper ocean circulation in the area of the spill, the shedding of the LCR from the LC, the circulation of the LCR, and the cyclonic circulation located to the northeast of the LCR (Fig. 1.1) that was partly responsible for advecting surface oil to the southeast during May and June (Figs. 1.4c, d and 1.7a). On June 28, the warm anticyclonic LCR started to detach for a second time (Fig. 1.4f). This LCR remained detached

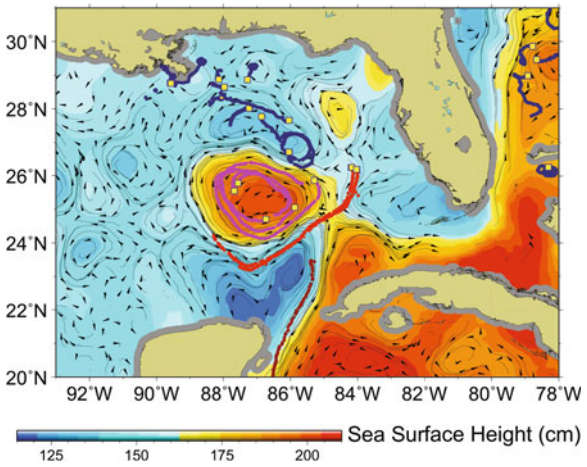

Fig. 1.8 Surface trajectories (coloured lines) of satellite-tracked drifting buoys ("drifters") between June 8–16. *Red lines* correspond to four drifters deployed during the Walton Smith research cruise [30] that served to assess the connectivity between the Loop Current and the Loop Current ring. *Purple lines* correspond to drifters that were used to monitor the circulation in the interior of the Loop Current eddy. *Black lines* correspond to drifters that served to monitor the ocean circulation to the northeast of the Loop Current ring. The background colours correspond to the altimetry-derived sea surface height while the *arrows* represent current vectors computed from the sea height field for June 13, 2010

until approximately August 1, 2010, when it reattached to the LC for a second time. Ultimately, only a small amount of surface oil was reported to have entered the northern LC/LCR system. Altimetry-derived observations show that this LCR, sometimes referred to as Eddy Franklin according to a naming protocol followed by some operational forecasters, eventually translated to the west and became undetectable early in 2011.

The scale of the DWH event required the use of satellite data to evaluate the impact of large oil spills on coastal and marine ecosystems. Satellite observations provided an important tool to conduct pre- and post-event evaluations of ecosystem processes. Current efforts are also focusing now on the investigation of the potential impact of oil on photosynthesis of plant species in the intertidal zone and of phytoplankton in offshore areas.

1.5 Conclusions

Hydrographic and satellite observations together with numerical model outputs played a key role in support of monitoring efforts during the DWH oil spill. The combined suite of observations and model outputs analysis can continually provide information about key parameters, such as ocean currents, frontal regions, water masses, and oil spill extent at the surface. This chapter presented important results on how the combined use of all available data and analysis were employed to monitor the surface oil areal extent and surface ocean currents in support of the restoration and recovery efforts, which were originally carried out under operational constraints involving short timelines and data resource availability.

Experimental Marine Pollution Surveillance (EMPS) reports, which provided an outer boundary of the extent of the surface oil, were used in this study to investigate the variability of the extent of surface oil using satellite imagery from both active and passive sensors and from supplementary information, such as overflights and in situ observations which were key for the assessment of numerical models. Results obtained from these reports show that the maximum surface area extent of the oil spill at the surface was approximately $47 \times 10^3\,km^2$, while the combined affected surface area was at least $130 \times 10^3\,km^2$. The oil spill surface extent exhibited large variability. The largest increase of surface oil occurred between April 22 and May 22, 2010, at an average rate of $1.3 \times 10^3\,km^2$ per day. On the other hand, the largest decrease in the extent of surface oil started on June 26, 2010, at an average rate of $4.4 \times 10^3\,km^2$ per day. The largest surface extensions ($>40 \times 10^3\,km^2$) occurred during several periods between late May and the end of June. The southernmost extension of the surface oil spill extent reached approximately 85°W 27°N during the beginning of June. Although smaller potential surface oil slicks were also identified to the south by MPSRs, only a few of them were observed from in situ and overflight observations, partly due to limited resources to evaluate them.

Real-time surface current fields derived from satellite altimetry were used to monitor conditions during the oil spill. In this work, delayed-time altimetry observations

were used to provide useful representations of the current fields. These observations, combined with the other satellite measurements and data from drifting buoys, provided a comprehensive view of the surface circulation dynamics. At the time of the oil spill, the core of the LC exhibited a northern extension (approximately 28°N), around 150 km from the oil spill site. At that time, this condition was hypothesized to have the potential of connecting waters, and probably oil particles, from the oil spill neighbouring areas into the central and southeastern GOM regions and beyond. Results obtained here indicate that surface currents, from the Loop Current, a Loop Current ring, and a cyclonic eddy, appeared to have controlled the southern and eastern extent of the surface oil during May and June. On the other hand, intense southeast winds associated with Hurricane Alex caused a reduction of the surface oil extent at the end of June and beginning of July, as oil was driven onshore and mixed underwater.

Results shown here represent a fraction of the combined DWH monitoring efforts and they clearly exemplify the key role that satellite observations and numerical model outputs play to monitor and analyse parameters critical for environmental studies at scales where in situ observations are not adequate or possible. For example, mesoscale features linked to the areal extent of surface oil confirm the important value of real-time eddy permitting satellite altimetry, along with SAR, IR and visible ocean colour data. This combination of active and passive satellite observations shows the utility of joint satellite data analysis for surface oil extent monitoring and studies. Although satellite observations serve to monitor surface parameters, in situ hydrographic observations and numerical modelling efforts are needed to obtain a subsurface assessment of the ocean conditions.

Results presented here also show the importance of extreme weather events in the oil spill areal extent, indicating that atmospheric ocean couple models may be necessary to properly monitor oil spacial extent.

Acknowledgments Funding for GG, JT, DS, and AMF was provided by NOAA. MJO was supported by NSF grant CMG0825547 and by a grant from BP/The Gulf of Mexico Research Initiative. JFM was partly funded by NASA grant NNX08AL60G, by a grant from BP/The Gulf of Mexico Research Initiative. We would also like to acknowledge the work of Mr. Gregory Gawlikowski (Roffer's Ocean Fishing Forecasting Service, Inc.) on mapping the distribution of oil and ocean frontal analyses, and to Dr. Francis Bringas for his support on numerical computations and distribution of fields of ocean currents through the NOAA/AOML web site. MAR was funded by Roffer's Ocean Fishing Forecasting Service, Inc., NASA Grant NNX08AL06G and University of Miami Cooperative Institute for Marine and Atmospheric Studies Grants NA10OAR432143 and R1100291, Florida Institute of Oceanography - University of South Florida grant 4710-1101-04. University of Miami CSTARS provided the SAR data. Altimetry sea height data are from AVISO. The information in this document reflects the views of the authors, and does not necessarily reflect the official positions or policies of the National Oceanic and Atmospheric Administration or the United States Department of Commerce.

References

1. Adcroft, A., Hallberg, R., Dunne, J.P., Samuels, B.L., Galt, J.A., Barker, C.H., Payton, D.: Simulations of underwater plumes of dissolved oil in the Gulf of Mexico. Geophys. Res. Lett. **37**, L18605 (2010). doi:10.1029/2010GL044689
2. Alpers, W., Espedal, H.A.: In: Jackson, Apel, (eds.) Synthetic Aperture Radar Marine Users Manual. NOAA NESDIS, pp. 262–276 (2004)
3. Emery, W.J., Strub, T., Leben, R., Foreman, M., McWilliams, J.C., Han, G., Ueno, H.: Satellite altimeter applications off the Coasts of North America. In: Vignudelli, S., Kostianoy, A., Cipollini, P., Benveniste, J. (eds.) Coastal Altimetry, pp. 417–451. Springer, New York (2011)
4. Goni, G.J., Johns, W.E.: A census of North Brazil current rings observed from TOPEX/POSEIDON altimetry: 1992–1998. Geophys. Res. Lett. **28**(1), 1–4 (2001)
5. Haller, G., Yuan, G.: Lagrangian coherent structures and mixing in two-dimensional turbulence. Physica D **147**, 352–370 (2000)
6. Hetland, D., Hsueh, Y., Leben, R., Niiler, P.: A loop current-induced jet along the edge of the West Florida Shelf. Geophys. Res. Lett. **26**, 2239–2242 (1999)
7. Hu, C., Nelson, J.R., Johns, E., Chen, Z., Weisberg, R.H., Muller-Karger, F.E.: Mississippi river water in the Florida Straits and in the Gulf Stream off Georgia in Summer 2004. Geophys. Res. Lett. **32**, L14606 (2005). doi:10.1029/2005GL022942
8. Hu, C., Li, X., Pichel, W.G., Muller-Karger, F.E.: Detection of natural oil slicks in the NW Gulf of Mexico using MODIS imagery. Geophys. Res. Lett. **36**, L01604 (2009). doi:10.1029/2008GL036119
9. Hulburt, H.E., Thompson, J.D.: A numerical study of loop current intrusions and eddy shedding. J. Phys. Oceangr. **10**, 1611–1651 (1980)
10. Klemas, V.: Tracking oil slicks and predicting their trajectories using remote sensors and models: case studies of the Sea Princess and Deepwater Horizon oil spills. J. Coast. Res. **25**, 789–797 (2010)
11. Lentini, C., Goni, G.J., Olson, D.: Investigation of Brazil Current rings in the confluence region. J. Geophys. Res. **111** (2000). doi:10.1029/2005JC002988
12. Lindo-Atichati, D., Bringas, F., Goni, G.: Loop Current Excursions and ring detachments during 1993–2009. Int. J. Remote Sens. **34**, 5042–5053 (2013)
13. Liu, Y., Weisberg, R.H.: Seasonal variability on the West Florida Shelf. Prog. Oceangr. **104**, 80–98 (2012). doi:10.1016/j.pocean.2012.06.001
14. Liu, Y., Weisberg, R.H., Hu, C., Kovach, C., Zheng, L.: Trajectory forecast as a rapid response to the deepwater horizon oil spill. In: Liu, Y., et al. (eds.) Monitoring and Modelling the Deepwater Horizon Oil Spill: A Record-Breaking Enterprise. Geophysical Monograph Series, vol. 195, pp. 153–165. AGU, Washington (2011). doi:10.1029/2011GM001121
15. Lugo-Fernandez, A.: Is the loop current a chaotic oscillator? J. Phys. Oceangr. **37**, 1455–1469 (2007)
16. Lubchenco, J., McNutt, M.K., Dreyfus, G., Murawski, S.A., Kennedy, D.M., Anastas, P.T., Chu, S., Hunter, T.: Science in support of Deepwater Horizon response. Proc. Natl. Acad. Sci. USA **109**, 20212–20221 (2012). doi:10.1073/pnas.1204729109
17. Macfadyen, A., Watabayashi, G.Y., Barker, C.H., Beegle-Krause, C.J.: Tactical modelling of surface oil transport during the Deepwater Horizon spill response. In: Liu, Y., Macfadyen, A., Ji, Z.-G., Weisberg, R.H. (eds.) Monitoring and Modelling the Deepwater Horizon Oil Spill: A Record-Breaking Enterprise. American Geophysical Union, Washington (2011). doi:10.1029/2011GM001128
18. Mariano, A., Kourafalou, V., Kang, H., Halliwell, G.R., Srinivasan, A., Ryan, E., Roffer, M.A.: On the modelling of the 2010 Gulf of Mexico Oil Spill. J. Dyn. Atmos. Oceans **52**, 322–340 (2011)
19. McNutt, M.K., Camilli, R., Crone, T., Guthrie, G., Hsieh, P., Ryerson, T.B., Savas, O., Shaffer, F.: Review of flow rate estimates of the Deepwater Horizon oil spill. Proc. Natl. Acad. Sci. USA **109**, 20260–20267 (2011). doi:10.1073/pnas.1112139108

20. Maul, G.A., Vukovich, F.M.: The relationship between variations in the Gulf of Mexico Loop Current and Straits of Florida volume transport. J. Phys. Oceanogr. **23**, 785–796 (1993)
21. Molinari, R.L., Mayer, D.A.: Current meter observations on the continental slope at two sites in the eastern Gulf of Mexico. J. Phys. Oceanogr. **12**, 1480–1492 (1982)
22. Muhling, B.A., Roffer, M.A., Lamkin, J.T., Ingram Jr, G.W., Upton, M.A., Gawlikowski, G., Muller-Karger, F.E., Habtes, S., Richards, W.J.: Overlap between Atlantic bluefin tuna spawning grounds and observed Deepwater Horizon surface oil in the northern Gulf of Mexico. Mar. Pollut. Bull. **64**, 679–687 (2012)
23. Muller-Karger, F.E., Walsh, J.J., Evans, R.H., Meyers, M.B.: On the seasonal phytoplankton concentration and sea surface temperature cycles of the Gulf of Mexico as determined by satellites. J. Geophys. Res. **96**, 12645–12665 (1991)
24. Muller-Karger, F.E.: The Spring 1998 NEGOM cold water event: remote sensing evidence for upwelling and for eastward advection of Mississippi water (or: How an Errant LC Anticyclone took the NEGOM for a spin). Gulf Mexico Sci. **1**, 55–67 (2000)
25. Oey, L.-Y., Ezer, T., Lee, H.C.: Loop Current, rings and related circulation in the Gulf of Mexico: a review of numerical models and future challenges. In: Sturges, W., Lugo-Fernandez, A. (eds.) Circulation in the Gulf of Mexico: Observations and Models, pp. 31–56. American Geophysical Union, Washington (2005)
26. Olascoaga, M.J.: Isolation on the West Florida Shelf with implications for red tides and pollutant dispersal in the Gulf of Mexico. Nonlinear Process. Geophys. **17**, 685–696 (2010)
27. Olascoaga, M.J., Haller, G.: Forecasting sudden changes in environmental pollution patterns. Proc. Natl. Acad. Sci. USA **109**, 4738–4743 (2012)
28. Olascoaga, M.J., Rypina, I.I., Brown, M.G., Beron-Vera, F.J., Kocak, H., Brand, L.E., Halliwell, G.R., Shay, L.K.: Persistent transport barrier on the West Florida Shelf. Geophys. Res. Lett. **33**, L22603 (2006). doi:10.1029/2006GL027800
29. Rio, M.H., Guinehut, S., Larnicol, G.: New CNES-CLS09 global mean dynamic topography computed from the combination of GRACE data, altimetry, and in situ measurements. J. Geophys. Res. **116**, C07018 (2011). doi:10.1029/2010JC006505
30. Smith, R. H., Johns, E. M., Goni, G. J., Trinanes, J., Lumpkin, R., Wood, A. M., Kelble, C. R., Cummings, S. R., Lamkin, J. T., Privoznik, S.: Oceanographic conditions in the Gulf of Mexico in July 2010, during the Deepwater Horizon oil spill. Cont. Shelf Res. **77**, 118–131 (2014). doi:10.1016/j.csr.2013.12.009
31. Shay, L.K., Jaimes, B., Brewster, J.K., Meyers, P., McCaskill, E.C., Uhlhorn, E., Marks, F., Halliwell Jr., G.R., Smedstad, O.M., Hogan, P.: Airborne ocean surveys of the loop current complex from NOAA WP-3D in support of the Deepwater Horizon Oil Spill. In: Liu, Y., et al. (eds.) Monitoring and Modelling the Deepwater Horizon Oil Spill: A Record-Breaking Enterprise. Geophysical Monograph Series, vol. 195, pp. 131–151. AGU, Washington (2011). doi:10.1029/2011GM001101
32. Streett, D.D.: NOAA'S satellite monitoring of marine oil. In: Liu, Y., Macfadyen, A., Ji, Z.-G., Weisberg, R.H. (eds.) Monitoring and Modelling the Deepwater Horizon Oil Spill: A Record-Breaking Enterprise. American Geophysical Union, Washington (2011). doi:10.1029/2011GM001104
33. Sturges, W., Leben, R.: Frequency of ring separations from the loop current in the Gulf of Mexico: a revised estimate. J. Phys. Oceanogr. **30**, 1814–1819 (2000)
34. Vukovich, F.M.: Climatology of ocean features in the Gulf of Mexico using satellite remote sensing data. J. Phys. Oceanogr. **37**, 689–707 (2007)
35. Yang, H., Weisberg, R.H., Niiler, P.P., Sturges, W., Johnson, W.: Lagrangian circulation and forbidden zone on the West Florida Shelf. Cont. Shelf Res. **19**, 1221–1245 (1999)
36. Zhang, H.-M., Bates, J.J., Reynolds, R.W.: Assessment of composite global sampling: sea surface wind speed. Geophys. Res. Lett. **33** (2006). doi:10.1029/2006GL027086
37. Zavala-Hidalgo, J., Morey, S.L., O'Brien, J.J., Zamudio, L.: On the loop current eddy shedding variability. Atmosfera **19**, 41–48 (2006)